HIGH DATA RATE PERFORMANCE OF A BCCD FOR RAPID SCAN IMAGING

David E. Schmieder and Stanley P. Buchanan
Martin Marietta Aerospace
Orlando, Florida

ABSTRACT

BCCD line arrays are very attractive for use in visual simulation and aerial mapping systems. However, to be most useful in these applications, it must be shown that such devices are capable of data rates to 16 MHz or higher and that they maintain high resolution and low noise operation at these higher rates. This paper discusses the results achieved when a commercially available 1728 element shallow bulk channel CCD line array is clocked at output data rates up to 30 MHz. The results show that temporal noise is near 200 electrons and is largely independent of clock rate. Charge transfer efficiency is found to be in excess of 0.9999 at 30 MHz.

I. INTRODUCTION

A. APPLICATIONS

Long, bulk channel CCD (BCCD) line arrays promise the capability to outperform area sensors in many applications which require low cost, but high resolution and jitter free imagery. This potential makes the BCCD line array very attractive for use in visual simulation and aerial mapping systems. For instance, visual simulation systems typically must cover wide fields of view at high resolution, often in a dynamic environment. Area sensors have difficulty meeting the resolution requirements and then often require video bandwidths above 80 MHz (Ref. 1). In addition, a dynamic environment smears the imagery due to the long 33 ms frame exposure periods. Solid state line sensors promise to overcome some of these problems with their higher resolution, potential for parallel operation, and shorter useful exposure periods. Similar benefits can be realized in aerial surveillance where the line array sensor can now replace film and provide real time imagery. The short exposure periods allow gimbal stabilization requirements to be relaxed and W/H effects to be minimized.

B. REQUIREMENTS

To be most attractive for these applications it is necessary to show that such devices are capable of high data rates and that they maintain high resolution and low noise operation. This is readily seen from a cursory examination of the data rates required in visual simulation. Here it is desired to provide wide 120° x 60° fields of view while maintaining resolution comparable to that of a human observer - near 1.5 arc minutes per resolution element. Interlaced frame rates should be no less than 30 frames/second to avoid flicker effects. The output sample rate (S) which corresponds to these requirements is simply.

$$S = \frac{(120 \text{ deg})(60 \text{ deg})(30 \text{ frames/sec})}{(1.5 \text{ arc min})^2 (1/60 \text{ arc min deg}^{-1})^2}$$

$$= 346 \text{ MHz}$$

Such data rates are well beyond the capabilities of a single vidicon or solid state sensor. But parallel operation of many side by side sensors can potentially provide this or even higher data rates. The difficulty is in achieving the focal plane sensor packaging density required for lower data rate sensor operation and low cost. The problems with packaging a vidicon for parallel operation are obvious. However, studies at Martin Marietta with the commercially available Fairchild Semiconductor 1728 element CCD line array (CCD121-DC) have shown that packaging densities of near 12 arrays per focal plane can be achieved in a scanning configuration with a reasonable focal plane size. This density then requires that each CCD line array be capable of output sample rates near 30 MHz. At this data rate the line exposure time is approximately

$$t_\ell = \frac{1728 \text{ elements}}{30 \text{ MHz}} \approx 60 \text{ µs.}$$

With such a short exposure time signal levels will be low and the utility of low noise as well as high speed operation is apparent.

A similar high speed, low noise operating requirement is apparent when the application of line arrays to aerial mapping is examined. In the past (Ref. 2) line arrays have been implemented in the "push-broom" configuration where vehicle motion is used to scan a continuous strip. The push-broom approach has generally not required high speed device operation but has required a complex optical system. The complexity has resulted when wide fields of view, combined with high resolution requirements, necessitated long focal planes of optically butted line arrays. An attractive alternative to the push-broom scheme in some applications is the "windshield wiper" implementation illustrated in Fig. 1. While this approach requires a moving gimbal to scan the array and a high device data rate, a single 1728 element line array can provide complete coverage over a wide field of view with a simple optical design.

The output data rates required in the windshield wiper scheme are exemplified by an aircraft operating at an altitude of 1200 feet and traveling at approximately Mach

0.6. The windshield wiper could be oriented to sweep out a wide 160° horizontal field while subtending 8° in the vertical direction. A continuous map of the ground would result if the array were scanned about once every 3.5 seconds with the gimbal oriented to scan the center of field at a down range distance of near 12 kft. The resolution provided would be a respectable

$$\frac{(8°)(17.4 \text{ mr/deg})(12 \text{ kft})}{1728} = 1 \text{ ft.}$$

However, the output data rate required of the 1728 element CCD array is high with a nominal requirement of:

$$\frac{(160°)(8°)(17.4 \text{ mr deg}^{-1})^2}{(3.5 \text{ sec})(1 \text{ ft}/12 \text{ kft})^2} \approx 16 \text{ MHz.}$$

This data rate corresponds to a "line" exposure time of approximately 110 μs and again points to the need for low noise operation if adequate signal to noise ratios are to be maintained.

These and other line array applications, such as helicopter obstacle avoidance, satellite surveillance, and laser beam pointing and tracking, potentially require the high resolution, high speed operation promised by large BCCD line arrays. This paper provides some of the data required to implement one such device at high data rates. Measured characteristics include noise levels, transfer efficiency, and resolution.

C. RESULTS SUMMARY

To date, commercially available, shallow bulk channel CCD line array characteristics have not been published for device operation above the 1-7 MHz regime (Refs. 2, 3). This paper presents the results achieved when a commercially available 1728 BCCD line array is clocked at output data rates up to 30 MHz. The more significant noise sources are identified; they include GCD (gated charge detector) reset noise, GCD thermal channel noise, and coherent clock pulse feedthrough. The results show that the total noise level from all sources is near 200 electrons and is nominally independent of clock rate. These results are shown to be in agreement with predictions.

Charge transfer efficiency and MTF (modulation transfer function) performance data are also presented for device operation at high data rates. Charge transfer efficiency is found to be in excess of 0.9999 at 30 MHz. This transfer efficiency allows high MTF performance.

II. DESCRIPTION OF THE 1728 ELEMENT ARRAY

Figure 2 shows a circuit representation of the 1728 element line array. This sensor was first described less than two years ago by C. K. Kim (Ref. 4). A complete description of the sensor can be found in the "Fairchild Charge Coupled Device · CCD 121" 1975 data sheet.* Some of the more significant device features are repeated here only to help in the understanding of the device performance data presented.

As shown in Figure 2, two 864 element, 2 phase, CCD shift registers are used to transport charge from the central photosites to a gated charge detector on-chip preamplifier. The photosites, spaced 13 μm apart, are separated by diffused channel stops and covered by a polysilicon photoelectrode.

In operation, charge packets from alternate photosites are transferred simultaneously to the CCD shift registers and clocked out. Interleaving, or recombining, occurs at the output gate to return the pulse train to its original sequence. Charge packets are detected in the GCD with a precharged diode whose potential changes in proportion to the quantity of charge delivered. This potential is applied to the gate of an output MOSFET (Fig. 2) which produces an output signal at OS. A reset FET is driven by a reset clock so as to recharge the diode capacitance before the arrival of each new charge packet from the transport registers. Operation of the GCD preamplifier is matched by a dumby compensation amplifier which provides an output similar in wave shape to the reset transient contained in the output signal. This compensation output can be used to partially cancel the rest transient in the video.

III. SPECIAL CONSIDERATIONS FOR OPERATION AT HIGH DATA RATES

A. INTERFACE, WAVEFORM, AND PHASING REQUIREMENTS

The major requirements for successful operation at rates up to 30 MHz were found to include:

1) Output rise and fall times of $\leq$ 10 ns on the output shift register drivers when loaded with 560 pf,

2) Driver output voltages of 0 to +12V with the low state to be held to no less than -0.4V to prevent charge injection into the substrate,

3) A 14V peak excursion on the GCD reset pulse with a 4 ns pulse width (at half maximum).

Selection and careful use of the National Semiconductor LH0033 Driver was sufficient to meet the above shift register requirements. Figure 3 shows oscilloscope pictures of the shift register drive waveforms produced by the LH0033 at a device output data rate of 30 MHz. It is to be noted that these waveforms more closely approximate a sine wave than the square wave being strived

*An improved version of this device has recently been introduced and called the CCD 121H.

for. This is an indication of the shift registers' insensitivity to drive wave shape. In fact, the sine wave was found to be preferable in that less clock pulse feedthrough was apparent in the output video than with sharper waveforms.

Other considerations for successful device operation at high data rates include provision for overall frequency stability and careful phase adjustment of the reset pulse.

B. CLOCK PULSE SUPPRESSION

The suppression of clock pulse coupling to the output video was found to be a major consideration at output data rates (f_c) above approximately 8 MHz. This coupling manifested itself in two forms: (1) GCD reset pulse feedthrough, and (2) digital logic transient coupling. The latter effect was most bothersome since it appeared as a fixed pattern noise at frequencies less than half the output data rate and thus occurred within the device's effective information passband. This noise source is discussed in more detail in section IV. Careful attention to board wiring consistent with good RF design techniques was the principal means used to reduce these effects. Reset pulse feedthrough was reduced to less than 5 mV relative to the advice's 170 mV maximum output with such techniques. It has been found that such reset pulse feedthrough, which occurs at the output clock frequency, can be reduced to insignificant levels when a lowpass filter with a sharp cut off at $f_c/2$ is employed in the video output circuit.

IV. MEASURED NOISE LEVELS

A. TEST SETUP

Figure 4 illustrates the sensor electrical operating configuration and output circuitry employed for high clock rate evaluation. Output circuitry operates the on-chip output MOSFET (Fig. 2) in a source follower configuration with a 1 kΩ load resistance (R_L). This produces a large current gain but results in a voltage gain of only 0.5. The voltage gain A_V is given by the expression

$$A_V = \frac{g_m R_L}{1 + g_m R_L} \qquad (1)$$

where g_m, the MOSFET transconductance, is 1 mmho. This configuration results in an output signal (at OS) saturation voltage (V_{SAT}) of approximately 170 mV when measured across Rl. Since the manufacturer claims that V_{SAT} corresponds to approximately 5×10^5 electrons per pixel, the amplifier charge detection responsivity at the device output is

$$Rq = \frac{5 \times 10^5 \text{ electrons}}{170 \times 10^3 \ \mu V} \qquad (2)$$

$$= 2.94 \text{ electrons}/\mu V$$

Output video is connected to the base of a buffer amplifier before being connected to the input of the first off-chip voltage boosting amplifier, the μA733. The buffer arrangement isolates the signal from loading effects of the μA733.

Noise measurements were made with an HP 8553B/8552B spectrum analyzer. This spectrum analyzer provides a CRT plot of the envelope detected rms noise level in a selectable measurement bandwidth swept over the frequency range from 0 to 100 MHz. The noise Wiener spectrum can be computed by squaring the rms CRT reading and dividing by the measurement bandwidth. Integration of the Wiener spectrum over frequencies from dc to $f_c/2$ is then the noise variance in the device's information passband. This measurement technique was felt to provide very accurate random noise measurement data when proper accounting for the spectrum analyzer's envelope detection scheme and the measurement bandwidth was made.

Coherent noise such as the fixed pattern variation in the output video, thought to be caused primarily by logic switching transients, could not be reliably measured with the spectrum analyzer. This coherent noise occurred at precise frequencies that were found to be harmonics of the various timing frequencies of the clock waveform generating logic. Coherent noise appeared as a periodic waveform. It was measured from scope trace photographs of the peak to peak variations in the output video averaged over many line periods.

Noise measurements were performed on a total of three CCD 121 sensors; no difference in noise level between devices, either temporally warying or fixed, was detected.

B. NOISE MEASUREMENT RESULTS

Temporal noise Wiener spectra due to all sensor and external circuit noise sources are presented in Figure 5 for various output clock rates f_c ranging from 4 to 30 MHz. These measurements were taken at room temperature with no input illumination on the sensor. The measurement system noise level, consisting of spectrum analyzer and video output circuitry noise, is also shown in the figure. The latter system noise was measured with the CCD 121 clocks and bias voltage inputs disabled. All noise values are related to the sensor output at OS in Fig. 4. The Wiener spectra noise densities are seen to fall rapidly past the frequency $f_c/2$. Spectral noise densities are also seen to decrease with increasing clock rate. This result is consistent with the dominant role played by GCD reset noise. Reset noise variance should be independent of output clock rate since the reset FET noise bandwidth is independent of the clock rate. Thus the noise Wiener spectra must, and do, show lower spectral noise densities as the bandwidth, over which this noise is distributed, increases.

Table 1 summarizes the rms noise levels per pixel which result from the previous noise spectra. Here off-chip output circuit and spectrum analyzer noise contributions have been removed. The noise densities are converted to a standard deviation in electrons per pixel by integrating the Wiener spectrum over frequencies from dc to $f_c/2$, obtaining the square root, and using the amplifier charge responsivity calculated in equation (2). These "temporal" noise magnitudes do contain a small (<12 electrons rms) fixed pattern noise due to dark charge variations as discussed in section V. Also shown in Table 1 are the predicted total rms temporal noise levels as computed from the noise models to be given in section V. Good agreement between measured and predicted noise levels indicates that the major noise sources have been correctly identified. Nevertheless, the consistently (∿10 percent) lower measured noise magnitude is an indication of either a slight systematic measurement error or over estimation in the noise prediction.

Table 1. Summary of measured temporal noise magnitudes, measured fixed pattern noise, and predicted temporal noise.

Output Bit Rate	4MHz	8MHz	16MHz	30MHz
Measured rms temporal[a] noise (electrons)	212	188	197	201
Predicted rms temporal[a] noise (electrons)	226	225	225	225
Measured rms fixed pattern noise[b] (electrons)	∿47	∿47	59	472
Total measured rms noise from all sources (electrons)	217	194	206	513

[a]Includes a small fixed pattern noise due to dark charge variations.
[b]rms = peak-to-peak/5

Finally, Table 1 indicates the measured fixed pattern noise found at the various output clock rates. This is believed to be primarily the result of either inductive or capacitive coupling of clock logic and driver transients to the output video. The drive and output circuitry employed in the test is seen to be susceptible to significant levels of fixed pattern noise at the higher clock rates. In principle this external noise source can be essentially eliminated, but to do so will require careful attention to proven RF design practices.

Figure 6 shows a representative noise spectrum for a 16 MHz output data rate as photographed from the CRT of the spectrum analyzer. The output data rate fundamental frequency can be clearly identified as can the line rate and line rate harmonics. Also clearly visible is an apparent coherent noise at $f_c/2$. This was found to be due to a slight difference in the shape of the reset feedthrough pulse between the two parallel shift registers shown in figure 2 and was not associated with a variation in the output video amplitude.

V. PREDICTED NOISE SOURCES AND MAGNITUDES

A. GCD RESET NOISE

The largest noise source in GCD type preamplifiers is due to the resetting of the precharged diode after each charge packet is shifted out. Thermal noise of the reset MOSFET channel resistance in parallel with the diode node capacitance (C) causes the amount of prechanging to vary each clock cycle. Thornber (Ref. 5) has shown this noise variance to be given by the expression:

$$N_r^2 \ (\text{electrons}^2) = \frac{2\ KTC}{3\ q^2} \qquad (3)$$

where

$K = 1.38 \times 20^{-23}$ (J/K°)

T = temperature (°K)

$q = 1.6 \times 10^{-19}$ (Coul/electron)

The node capacitance can be determined from the relation:

$$C = \frac{q\ N_{SAT}\ G_V}{V_{SAT}} \qquad (4)$$

where

N_{SAT} = pixel saturation charge (∿5 x 10^5 electronics)

V_{SAT} = saturation output voltage (∿0.170V)

G_V = voltage gain at output (0.5)

Hence:

C = 0.23 pf.

Thus at 300°K the rms thermal noise of the reset MOSFET is

N_r = 157 electrons

However, both the signal GCD and the compensation GCD show reset noise. Since these noise sources are uncorrelated and combined in the μA733 amplifier (Fig. 4) they must be added in quadrature giving a total rms reset noise level of

N_r (total) = 223 electrons

B. OUTPUT MOSFET NOISE

The output noise (Ref. 6) of the on-chip MOSFET preamplifier consists of thermal

noise of the channel resistance and a thermal noise due to an effective shunt resistance between gate and source. At high clock rates ($\geq$ 1 MHz) the latter (Ref. 7) parallel resistance can be neglected. The expression for channel resistance thermal noise variance is

$$N_t^2 = \frac{4\ KT\ R_s\ \Delta f\ C^2}{q^2} \qquad (5)$$

where, from Reference 6, $R_s \simeq (2/3)\ (1/gm)$. Thus for a bandwidth Δf of half the output clock frequency $f_c/2$ = 15 MHz, and g_m = 1 mmho, the RMS thermal noise is N_t = 19 electrons. Addition of this amount in quadrature with that from the compensation GCD indicates a total rms thermal channel noise of N_t = 27 electrons.

C. BULK TRAPPING NOISE

Bulk channel CCD's show a signal fluctuation due to the filling and emptying (Ref. 8) of bulk states as the signal transfers along the channel. For a single level of bulk traps with density N_{tk} and interacting volume V_c per pixel the maximum variance associated with this transfer noise was shown (Ref. 7) to be

$$N_b^2 = 0.25\ V_c\ N_{tk} \qquad (6)$$

The magnitude of N_{tk} was indicated by Jack and Dyck (Ref. 9) to be consistent with a single level trap density near 1 x 10^{11} cm^{-3}. Volume V_c occupied by the signal packet at low signal levels will be at least an order of magnitude less than the volume of the pixel. The latter is that of a 13 µm x 17 µm area with a buried channel depth of approximately 1/4 to 1/2 µm (Ref. 10). Therefore the maximum signal packet volume should be no greater than 1.1 x 10^{-10} cm^3 and for small signal levels would be less than 10^{-11} cm^3. It is readily seen from equation (6) that bulk trapping noise levels are predicted to be insignificant.

D. DARK CURRENT SHOT NOISE

Thermal dark charge generation in CCD photosites and transfer registers gives rise to a dc background level. The generation process is random and known to obey Poisson statistics. Hence, the rms dark charge temporal noise can be thought of as a shot noise equal to the square root of the mean charge level. The average background charge N_d was measured at a 1 MHz output rate to be 5000 electrons per pixel at room temperature. Hence the dark level at output frequency f_c is nominally:

$$N_d = \frac{5000}{f_c\ (MHz)} \qquad (7)$$

The dc charge at 30 MHz is then 167 electrons and the associated rms shot noise is 13 electrons.

E. FIXED PATTERN NOISE

Fixed pattern, or temporally non-varying, noise has been found to originate from four potentially bothersome sources. These are non-uniformities in the dark charge generation rate, photoresponse non-uniformity, GCD reset pulse feedthrough, and clock pulse generation logic transients. The latter two can, in principle, be held to low levels.

Dark charge non-uniformity, according to the manufacturer's data sheet is typically 3 percent of saturation or ∿15000 electrons (zero-to-peak) at room temperature after a 1.94 ms integration time. Measured non-uniformities were much less and were found to be primarily manifested as a gradual change in the dc level across the array. Random dark charge variation between pixels was approximately 48 electrons rms at 1 MHz (1.94 ms integration time). This corresponds to ∿1 electron with the ∿60 µs integration time available at a 30 MHz clock rate. Only the random variations are believed to effectively contribute to the overall rms noise level.

Photoresponse non-uniformity is claimed to be typically $\pm$6 percent of the signal level. Thus the final fixed pattern noise contribution from this source will depend upon the actual signal level available. Measurements on two devices have shown non-uniformities of $\pm$3 percent with broadband irradiance but $\pm$10 percent with 0.86 µm narrowband irradiance. This non-uniformity will generally not contribute a significant amount of fixed pattern noise under low light level operating conditions.

Table 2 shows a summary of the predicted noise from the various noise sources for f_c = 30 MHz. The total rms total noise of 225 electrons is clearly dominated by GCD reset noise. If this noise could be eliminated by the process of correlated double sampling (Ref. 11), without a large implementation noise penalty at these high clock rates, the total noise level could be reduced to significantly lower levels. Likewise, reduction of the reset node capacitance, already accomplished in the new CCD121H (Ref. 10) line array, is expected to produce a much reduced noise level.

Table 2. Noise source contributions (rms electrons) at f_c = 30 MHz

GCD Reset	Output MOSFET	Bulk Trapping	Dk. Chg. Shot	Dk. Chg. Fixed Pat.	Total
223	27	∿0	13	∿1	225

VI. CHARGE TRANSFER EFFICIENCY

A. MEASUREMENT APPROACH

Efforts to measure charge transfer inefficiency were made for CCD121 operation

at clock rates up to 30 MHz. The measurement technique consisted of focusing a HeNe CW laser on a single pixel of the array and measuring the charge lost to trailing charge packets in the output shift register. Charge levels employed in these tests were in the range from 50 to 100 percent of pixel saturation. Although the laser spot size employed in was only slightly less than the pixel center-to-center spacing, potential difficulties from spot spillover or diffusion, which could lead to erroneous results, were not encountered due to the devices alternate photosite transfer technique (Fig. 2). With this technique alternate sites are shifted to different output registers, hence spillover due to transfer inefficiency can occur only in alternate charge packets in the output data. This fact helps to distinguish transfer inefficiency effects from other spurious effects.

B. RESULTS

The experimental apparatus employed for transfer inefficiency measurements was too insensitive to measure the small inefficiencies encountered at $f_c < 30$ MHz. At 30 MHz, however, an $\eta\epsilon$ product of $\simeq 0.09$ was measured after 1330 transfers. Here $\eta\epsilon$ is the usual measure of transfer inefficiency where η is the number of transfers and ϵ is the fraction of charge not transferred per shift. The resulting transfer efficiency $(1-\epsilon)$ for the above $\eta\epsilon$ product is 0.99993. Figure 7 shows a photograph of the oscilliscope trace for the output pixel train at 30 MHz containing single pixel illumination.

In the process of arriving at a waveform for driving the CCD121 at high clock rates the authors measured transfer efficiencies much lower than the above. It was concluded that $\eta\epsilon$ is very sensitive to driving waveform shape and voltage swing. The shift register waveforms used for the above measurement are shown in figure 3. The present experimental results to not preclude the possibility that still higher transfer efficiencies can be obtained for different driving waveforms.

VII. MTF PERFORMANCE

In order for this sensor to be useful at high data rates it is important that the device maintain high resolution as well as low noise. High transfer efficiency, as reported in the previous section, should provide resolution comparable to that available at lower clock rates. The measurements reported in this section support that conclusion at a data rate of 30 MHz.

A. APPROACH

The objective of resolution performance measurements here is to obtain an estimate of the CCD121's sine wave response at the output data rate of 30 MHz. While the square wave response is much easier to measure, it is awkward for the system designer to use when attempting to predict the combined performance of many cascaded subsystems. The normal procedure is to measure square response and then simply transform it to a sine wave response. The problem with using this approach is that the transform requires accurate square wave response data at frequencies several multiples higher than the frequency of interest. With sampling devices, such as CCD's, response data above the basic Nyquist limited spatial sampling rate is ambiguous. Its use in the transform would likely lead to an ambiguous conclusion. To skirt this problem a reverse approach is taken. The BCCD's sine wave response is first predicted from basic principles, the sine wave response is transformed to a square wave response, and finally, the predicted square wave response is compared to measured square wave response data.

B. PREDICTED SINE WAVE RESPONSE

The sine wave response can be computed for a sampled CCD image plane by assuming the individual receiving apertures (pixels) are always geometrically aligned with a sine wave input pattern to obtain the maximum amplitude response. This amplitude response at any given spatial frequency is the device's "in-phase" Modulation Transfer Function (MTF). The term Modulation Transfer Function is defined here as the amplitude of the optical transfer function (OTF) and can assume negative values. The MTF is converted to a square wave response (H_{sq}) at spatial frequency v by the relationship (Ref. 12)

$$H_{sq}(v) = \frac{4}{\pi}\left[MTF\ (v) - \frac{MTF\ (3v)}{V} + \frac{MTF\ (5v)}{5} - \ldots\right] \qquad (8)$$

The MTF of the 1728 element BCCD is predicted from the individual response functions of three known resolution degrading phenomena. These include the response (M_a) due to a finite aperture, the response (M_t) due to transfer inefficiency and the response (M_d) due to carrier diffusion in the substrate. The one dimensional aperture response is given by the well known relation

$$M_a = \frac{\sin \pi dv}{\pi\ dv} \qquad (9)$$

where d is the pixel aperture size (13 μm). Joyce and Bertrum (Ref. 13) have determined that the response due to transfer inefficiency can be expressed as

$$M_t = (1-\epsilon)^{n_e}\ \eta\epsilon\ \cos(2\ \pi v/N_p) \qquad (10)$$

where Np is the device's spatial sampling frequency (76.9 pixels/mm). Figure 8 shows a plot of the aperture function and transfer inefficiency response for n = 1040 transfers and $\epsilon = 0.99993$. Finally Sieb (Ref. 14) has shown that the response function due to charge carrier diffusion is

$$M_d = C\left(1 - \frac{e^{-\alpha L_D}}{1 + \alpha L}\right) \qquad (11)$$

where

C = normalization constant,

α = optical absorption coefficient of silicon,

L_D = depletion width

$$L = \left(\frac{L_o^2}{1+L_o^2 K^2}\right)^{1/2}$$

L_o = diffusion length

$K = 2\pi \nu$ (lp/mm)

The M_d expression is also plotted in figure 8 for an α characteristic of silicon at a wavelength of 0.862 μm and at 300°K taken from reference 15. This wavelength was selected to correspond with the measurements taken with a narrow bandpass filter centered at 0.862 μm. The other parameters were assumed as follows:

$L_D \simeq 0.01$ mm

$L_o \simeq 0.1$ mm

per values indicated in reference 16 for BCCD devices of similar architecture. Figure 8 shows a plot of the total resulting CCD121 sine wave response as predicted from the relation

$$MTF = M_a \cdot M_t \cdot M_d \qquad (12)$$

C. MEASURED SQUARE WAVE RESPONSE

The 1728 element BCCD square wave response was measured by imaging a standard 4 bar, 7:1 aspect ratio resolution chart on the array through an f2.5 Angenieux lens. Chart illumination was filtered with a 0.03 μm bandpass filter centered at 0.862 μm. The lens MTF was measured on an Optics Technology model K-III MTF analyzer with a 0.09 μm bandpass filter. This, slightly larger lens measurement passband tended to under rate the lens MTF actually available in the CCD resolution tests by a small amount. Figure 9 shows the measured lens MTF, the predicted CCD121 MTF from figure 8, and their product. This combined MTF, when transformed to a square wave response, should compare to the measured square wave response data.

Figure 10 illustrates the combined CCD121 and test lens measured square wave response at 30 MHz and the corresponding predicted square wave response as computed from equation (8). It is seen that the predicted response compares favorably with measured data. This favorable comparison supports the use of the CCD121 MTF shown in figure 8 as the device's sine wave response up to the cutoff frequency of 38.4 lp/mm for the stated conditions.

VIII. SUMMARY AND CONCLUSIONS

Long CCD line arrays are believed to promise advantages over area type sensors in several applications. These include flight simulation and aerial surveillance. To be suitable for these applications in the implementation schemes presented it must be shown that the long line arrays maintain low noise levels and high resolution when clocked at output data rates to 30 MHz. Results presented in this paper show that a commercially available 1728 element bulk channel CCD line array does indeed meet these requirements.

ACKNOWLEDGEMENT

The authors wish to acknowledge the contributions of Mr. Henry E. Helms of Martin Marietta Aerospace whose circuit design expertise led to successful CCD121 operation at high data rates. They also wish to thank Drs. David D. Wen and Rudolph H. Dyck of Fairchild Semiconductor for their helpful discussions and device operating suggestions.

REFERENCES

1. Irish, Kenneth M., et. al., "Visual Simulation Video Processing Techniques," AFHRL-TR-74-76. p.25, December, 1974.

2. Vicars-Harris, M., "Slow-Scan Operation of Long Linear CCD Arrays," Proceedings of the Symposium On Charge-Coupled Device Technology for Scientific Imaging Applications, Pasadena, CA., March 1975.

3. Hunt, J, and Sadowski, H., "Diverse Electronic Imaging Applications for CCD Line Image Sensors," Proceedings of the 1975 International Conference on the Application of Charge-Coupled Devices, San Diego, CA., October 1975.

4. Kim, C. K., "Two Phase Charge Coupled Linear Imaging Device with Self-Aligned Implanted Barrier," IEDM Technical Digest, December 1974.

5. Thornber, K. K., "Noise Suppression in Charge Transfer Devices," Proc. IEEE, Vol. 60, P. 1113, 1972.

6. Motchenbacker, C. and Fitchen, F., Low Noise Electronic Design, John Wiley and Sons, Inc. 1973.

7. Sequin, C. H., and Tompsett, M. F., Charge Transfer Devices, Academic Press, 1975.

8. Moshen, A. M., and Tompsett, M. F., "The Effects of Bulk Traps on the Performance of Bulk Channel Charge-Coupled Devices," IEEE Trans. on Elec. Devices, Vol. ED-21, No. 11, Nov. 1974.

9. Jack, M. D., and Dyck, R. H., "Charge-Transfer Efficiency in a Buried-Channel

Charge-Coupled Device at Very Low Signal Levels," IEEE Trans. on Elec. Devices, Vol. ED-23, No. 2, Feb. 1976.

10. Wen, David D. Private Communication, July 8, 1976.

11. White, M. H., et. al., "Characterization of Surface Channel CCD Image Arrays at Low Light Levels," IEEE Journal of Solid State Circuits, Vol. SC-9, No. 1, Feb. 1974.

12. Coltman, John W., "The Specification of Imaging Properties by Response to a Sine Wave Input," JOSA, Vol. 44, No. 6, June 1954.

13. Joyce, W. B., and Bertrum, W. J., "Linearized Dispersion Relation and Green's Function for Discrete-Charge-Transfer Devices with Incomplete Transfer," BSTJ, Vol. 50, No. 6, July-August 1971.

14. Sieb, David, "Carrier Diffusion Degradation of Modulation Transfer Function in Charge Coupled Imagers," IEEE Transactions on Electron Devices, Vol. ED-21, No. 3, March 1974.

15. Dash, W. C., and Newman, R., "Intrinsic Optical Absorption in Single-Crystal Germanium and Silicon at 77°K and 300°K," Physical REview, Vol. 99, No. 4 August 15, 1955.

16. "Low Light Level Charge-Coupled Imaging Devices (Phase I)" Final Report, Oct. 1973, AD915 544L.

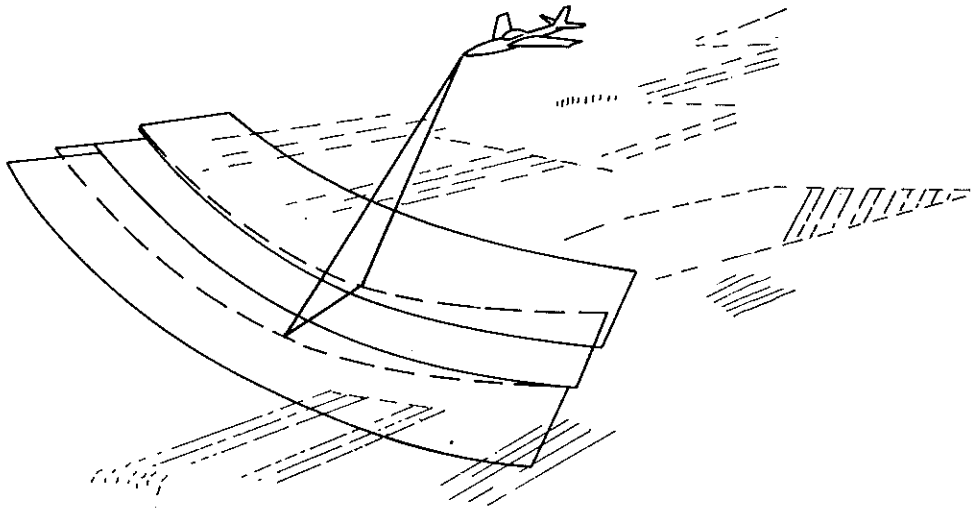

Fig. 1. Illustration of "windshield wiper" scan pattern in aerial mapping.

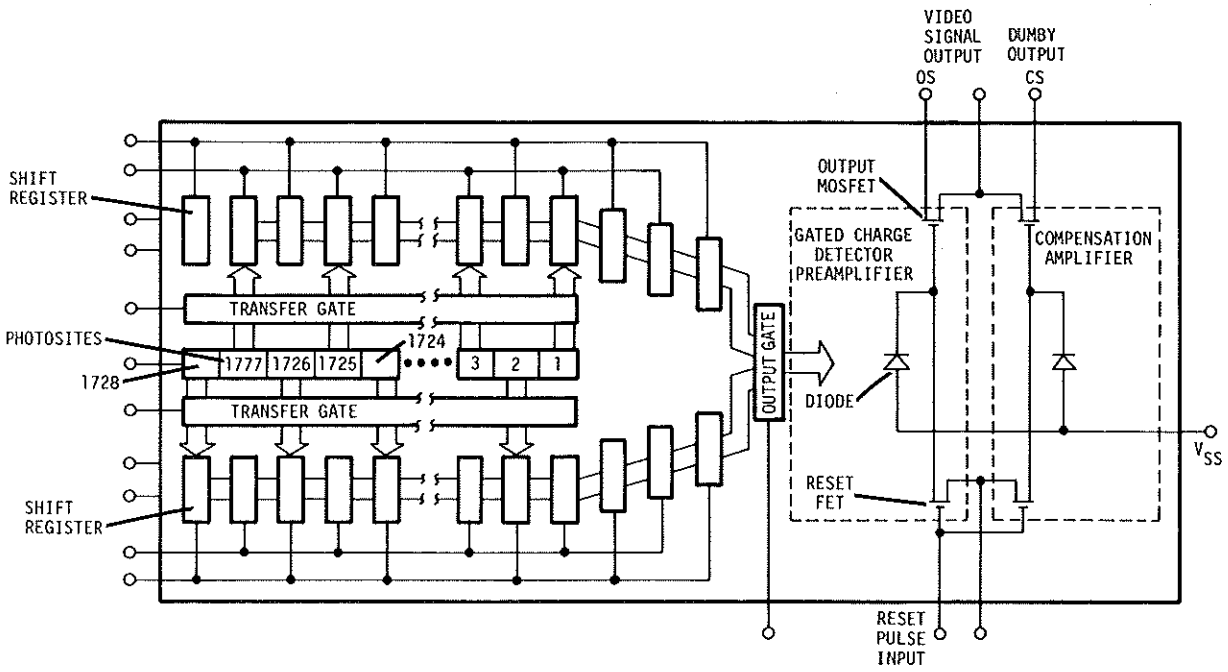

Fig. 2. CCD 121 circuit representation

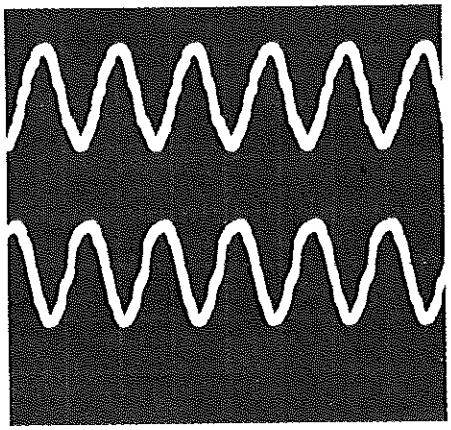

Fig. 3. Driver waveforms supplied to one of the two phase, parallel output shift registers at 30 MHz output data rate when loaded with 560 pf capacitance. Vertical scale is 5V/div, horizontal scale is 50 ns/div, scope bandwidth is 150 MHz.

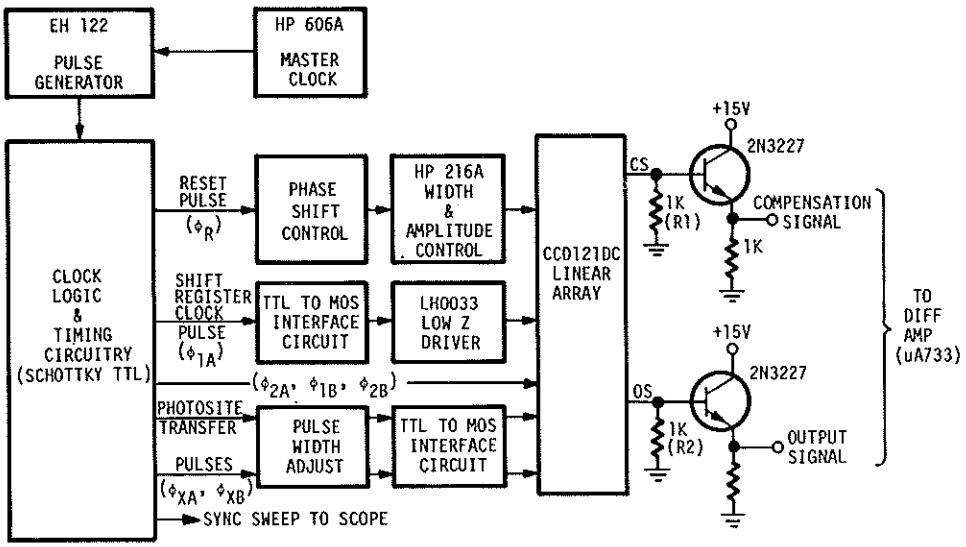

Fig. 4. Line array drive configuration and output circuitry for high speed evaluation.

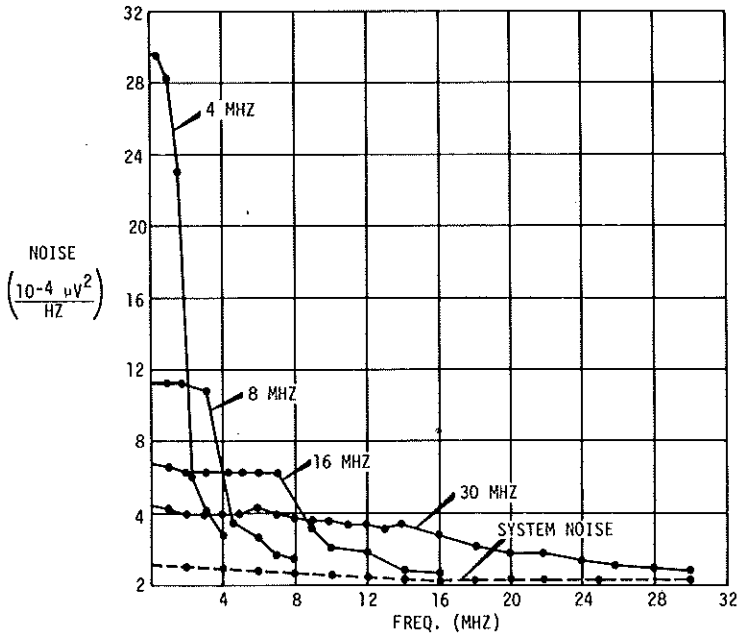

Fig. 5. Wiener spectra of CCD 121 and measurement circuit temporal noise for various output data rates.

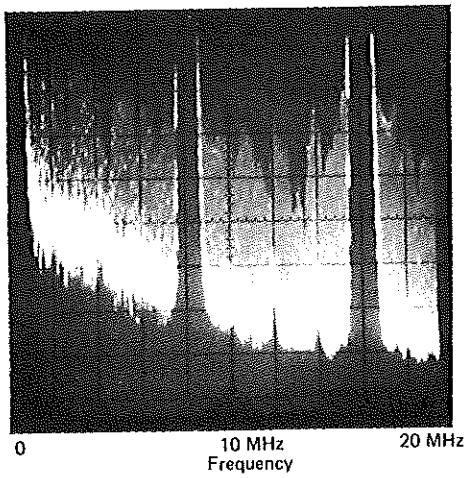

Fig. 6. Representative noise spectrum display at a 16 MHz output data rate. Scale is 20 μv/div vertical and 2 MHz/div horizontal. System gain is 5.0. Evidence of fixed pattern noise at frequencies $<f_c/2$ can be seen at 2 and 4 MHz.

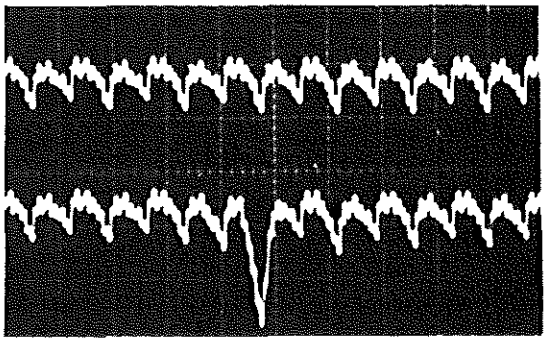

Fig. 7. Output wave train from CCD 121 at 30 MHz with an offset between the parallel output registers. The top trace shows output with no input illumination on the device. The bottom trace shows pixel number 1330 illuminated with some stray light falling on the preceding pixel. (Scale: 0.2 V/div vertical, 50 ns/div horizontal).

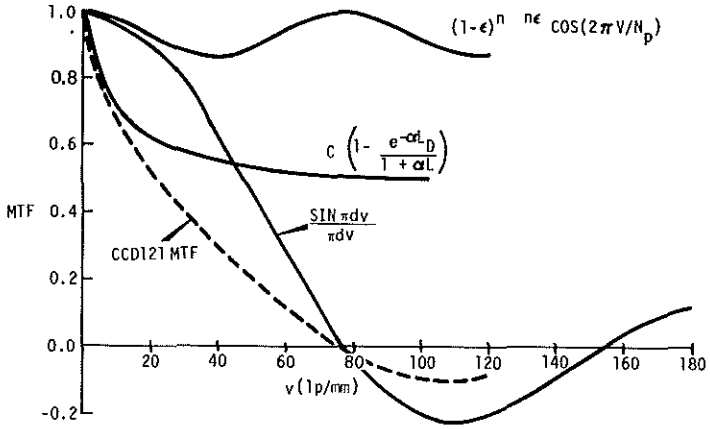

Fig. 8. Plot of total CCD 121 MTF and constitutent response functions for a 30 MHz clock rate and 0.862 um narrowband illumination.

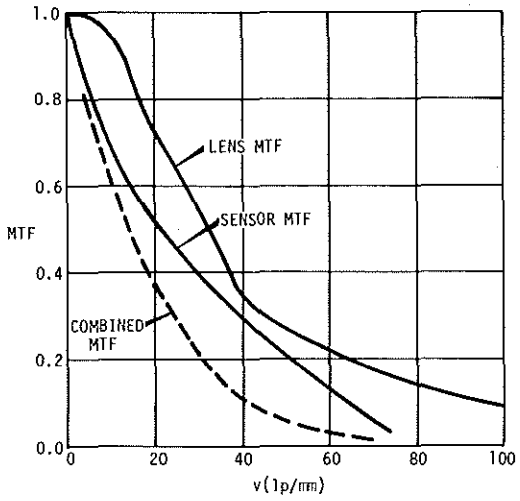

Fig. 9. Measured test lens MTF and combined sensor and lens MTF response.

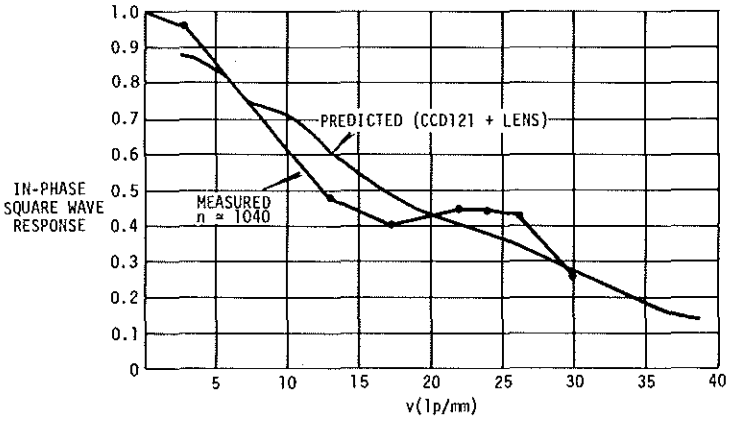

Fig. 10. Comparison of predicted and measured square wave response for a clock rate of 30 MHz and narrowband illumination centered at 0.862 μm.